A Study on the Plasmonic Properties of Silver Core Gold Shell Nanoparticles: Optical Assessment of the Particle Structure

Derrick Mott*, JaeDong Lee, Nguyen Thi Bich Thuy, Yoshiya Aoki, Prerna Singh, and Shinya Maenosono

School of Materials Science, Japan Advanced Institute of Science and Technology, Nomi, Ishikawa 923-1292, Japan

Received:

*E-mail: derrickm@jaist.ac.jp

This paper reports a qualitative comparison between the optical properties of a set of silver core, gold shell nanoparticles with varying composition and structure to those calculated using the Mie solution. To achieve this, silver nanoparticles were synthesized in aqueous phase from a silver hydroxide precursor with sodium acrylate as dual reducing-capping agent. The particles were then coated with a layer of gold with controllable thickness through a reduction-deposition process. The resulting nanoparticles reveal well defined optical properties that make them suitable for comparison to ideal calculated results using the Mie solution. The discussion focuses on the correlation between the synthesized core shell nanoparticles with varying Au shell thickness and the Mie solution results in terms of the optical properties. The results give insight in how to design and synthesize silver core, gold shell nanoparticles with controllable optical properties (e.g., SPR band in terms of intensity and position), and has implications in creating nanoparticle materials to be used as biological probes and sensing elements.

1. Introduction

To date, Ag and Au nanoparticles (NPs) have become exciting nanoscale probes for the detection of a wide range of biomolecules including proteins,[1)] amino acids,[2)] antibodies/antigens,[3)] DNA,[4)] and others.[1,2)] These nanoscale probes offer enhanced detection limits and sensitivities over conventional detection techniques because of the enhanced properties that emerge as a result of the nanoscale size.[1,5)] In the field of biomolecular detection, Ag NPs have been demonstrated to possess one of the highest Raman activities so far documented,[6)] while Au NPs have been used because of the stability (resistance to oxidation, etc) and to take advantage of the strong Au-thiol interaction.[2,4,7)] In light of both the advantages and disadvantages encountered in the individual Ag and Au metal NPs, the desire to couple the metals into a single functional probe has emerged.[8-10)] Silver core gold shell (Ag@Au) NPs have become intriguing biological probes in the field of sensing and diagnostics because of the beneficial coupling of the two metals.[3,4)] The Ag core provides enhanced Raman activity[3,4,11)] while the Au shell provides stability (resistance to oxidation, etc) and a beneficial reactivity with sulfur containing biomolecules.[2-4)] Several researchers have devised techniques to synthesize Ag@Au NPs for biological sensing applications. Some notable techniques include those by Cao *et al.* who first synthesized Ag NPs using the citrate reduction method, then grew Au on the surface of the Ag NPs by simultaneous addition of $HAuCl_4$ and $NaBH_4$ solutions,[4)] Cui *et al.* and Srnová-Šloufová *et al.* both independently prepared Ag@Au NPs by growing gold on the surface of Ag NPs using $HAuCl_4$ precursor and $NH_2OH{\cdot}HCl$ as reducing/deposition agent,[3,12)] and Yang *et al.* prepared Ag@Au NPs by transferring Ag NPs to toluene, adding $AuCl_4^-$, and allowing the Au to oxidize the Ag surface until a complete shell of Au was formed.[13)] In our own research, we have developed a technique towards Ag@Au NPs where the Ag cores are synthesized using sodium acrylate as a co-reducing/capping[14)] agent and the gold is grown on the Ag surface by simultaneous addition of $HAuCl_4$ and additional sodium acrylate at reflux.[15)] Many of the synthesized Ag@Au probes mentioned above have found use in the

ultra-sensitive detection of specific biomolecules including DNA[4] and antibody/antigens,[3] which illustrates the potential of these probes to be routinely used in clinical settings for biomolecular detection.[1] Despite these advances however, there is still a lack in understanding of the correlation between the size, shape, composition and structure properties of the Ag@Au NPs and the resulting optical properties. For example, is a surface plasmon resonance (SPR) band expected for each component metal, or is a single intermediate band expected?[16,17] One of the most useful tools that has developed for studying the optical properties for nanosized particles is the use of the Mie solution to model the ideal optical behavior.[16,18] There have been several reports on the optical property modeling of a wide range of nanoscale materials, most notably for Ag,[19,20] Au,[5,21] Ag-Au alloys,[17,18,22] and Ag@Au,[16,17] and a general understanding of the resulting optical properties for these materials has been achieved.[23] However, in most cases the Mie solution has been applied to ideal systems where particle size, shape, structure and composition are completely uniform. In cases where non uniform Ag@Au NPs have been created in terms of structure, the Mie solution has found less use. As the NP structure becomes increasingly more complex, so too does the modeling of the expected optical properties. For the synthesis of Ag@Au NPs mentioned above, few techniques could achieve completely uniform particles in terms of composition[12] or structure.[3] Indeed many instances showed NPs with gaps or defects at the surface[3] which complicates the analysis of the optical properties, because the Mie solution explicitly applies to an ideal system (i.e., a Ag core completely encapsulated in a uniform layer of Au). The aim of this paper is to employ the Mie solution as an aid to understanding the optical properties of a set of Ag@Au NPs with non uniform structure, which has not been done before. In our synthesis technique we demonstrated the formation of Ag@Au NPs with defects in the structure such as gaps in the Au shell, or partial etching of the silver core.[15] Here, the Mie solution is applied to this non ideal system to gain an understanding of the structural parameters for Ag@Au NPs that give rise to the experimentally observed optical properties. The Mie solution is employed in such a way as to reflect the optical properties for

Ag@Au NPs with non ideal structures, expanding the use of the Mie solution outside the realm of completely uniform and ideal materials. This study has two purposes, the first is to analyze the optical properties for a set of structurally non-uniform Ag@Au NPs in terms of the shape/position of the surface plasmon resonance (SPR) band. The second is to qualitatively correlate the calculated optical properties to the experimentally determined ones so that the structure of the synthesized NPs may be inferred. In this research work the synthesis and characterization of the Ag@Au NPs is briefly presented as the full discussion has been reported previously.[15] Ultimately, the understanding of the complex structural-optical properties gives insight in how to create nanoprobes with desired optical properties by controlling the materials size, composition, structure and other parameters.

2. Experimental Methods

2.1 Chemicals

Silver nitrate, sodium acrylate, gold tetrachloroaurate trihydrate and common solvents were obtained from Aldrich. Water was purified with a Millipore Direct-Q system (18.2 MΩ). Dialysis membranes with molecular weight pore size of 10,000 Daltons were obtained from Spectra/Por and were rinsed in pure water before use.

2.2 Synthesis of Ag NP cores

Ag NPs were synthesized by first dissolving 1.25×10^{-5} moles of silver nitrate into 50 ml of water, and then adding 6.75×10^{-6} moles of sodium hydroxide, which results in a dilute yellow colored solution. This solution is purged with argon and is then brought to reflux. At reflux, 2.55×10^{-4} moles of sodium acrylate are added causing the solution to turn completely clear. The solution is refluxed for 1 hour, over this time the solution color changes from clear to green-yellow to yellow-orange.[15]

2.3 Purification of as-synthesized Ag NPs

Prior to deposition of Au on the Ag NP seeds, the as-synthesized particles are purified to

remove excess acrylate, silver, sodium, and other ions from the solution. Purification is performed by encasing the particle solution inside a cellulose dialysis membrane with pore size of 10,000 Da and soaking in a distilled water bath. The water was changed every 12 h for 48 h.[15)]

2.4 Deposition of Au on the Ag cores to form Ag@Au NPs

Fifty milliliters of the dialysized Ag particles are brought to reflux and 10 ml of a gold tetrachloroaurate trihydrate solution (ranging from 6.25×10^{-7} to 3.13×10^{-6} moles according to the thickness of the Au shell desired) and 10 ml of a sodium acrylate solution (from 5.10×10^{-5} to 2.55×10^{-4} moles) are added dropwise simultaneously. The degree of solution color change depends on the amount of Au added. In general, as Au and sodium acrylate is added to the Ag particles, the color changes from yellow-amber to dark amber to grey to grey-purple and finally to purple.[15)]

2.5 Mie solution

The calculation is based on the Mie solution for nanosized metallic spheres placed in water (dielectric constant = 1.77). In the solution, the metallic dielectric function $\varepsilon(\omega) = 1-\omega_p^2/\omega(\omega+i\gamma)$ for the sphere is incorporated, where ω_p is the plasmon frequency depending on the specific metal. The Drude model was used to determine the dielectric function of the different metals used in the study. The Drude parameters used include the plasmon frequency and the peak broadening for each metal (i.e., Ag and Au). The plasmon frequencies used for Ag and Au are 6.46 and 5.07 eV, respectively. The peak broadening used does not include quantum size correction and was chosen based on fitting the modeled curves to the experimentally determined ones. The peak broadening used for Ag and Au was 0.65 and 1.5 eV, respectively. In terms of the nanoparticle size used in the calculation, our interest is primarily in the absorption spectral "shape" between theory and experiment, so the size of the overall nanoparticle is not definitively defined in the model (the absorption strength is proportional to R^3, where R is the radius of the overall nanoparticle), instead the particle size is inherently

incorporated in the dielectric constant used (i.e., the plasmon frequencies used align with those experimentally observed). Because the overall radius is not so important for the absorption spectral "shape", our approach still stands even though the size distributions of our NPs are somewhat broad. The most important parameters in the calculation are the relative thickness of the shell, size of the core, and the overall particle structure. In general, three different structural models were studied with this approach. The models are used to represent realistic structures for different compositions of Ag@Au NPs and are described more fully in the text.

2.6 Instrumentation and measurements

Techniques including transmission electron microscopy (TEM), energy-dispersive spectroscopy (EDS), X-ray photoelectron spectroscopy (XPS), and ultraviolet visible spectroscopy (UV-vis) were used to characterize the size, shape, composition and other properties of the NPs. TEM analysis was performed on a Hitachi H-7100 transmission electron microscope operated at 100 kV. EDS was performed on a Hitachi H-9000NAR transmission electron microscope operated at 300 kV. The nominal spot size for EDS analysis of single NPs was ~25 nm in diameter. TEM and EDS samples were prepared by dropping the suspended particles onto a carbon coated copper grid and drying overnight in air. HR-TEM/EDS Mapping were conducted on a JEOL JEM-ARM200F scanning TEM (STEM) operated at 200 kV with Ag L and Au M lines used for the mapping analysis. XPS spectra were collected using a Physical Electronics ESCA 5600 multi-technique XPS system. Samples of suspended NPs were dropped onto conductive carbon paper and allowed to dry overnight. The nominal spot size for XPS analysis was 2.5×10^5 μm^2. UV-vis spectra were collected in the range of 300 to 1100 nm using a Perkin-Elmer Lambda 35 UV-vis spectrometer.

3. Results

Ag NPs as well as three samples of Ag@Au with increasing Au shell thickness were prepared according to the procedure described above. The gold shell thickness was varied by

changing the amount of gold precursor used in the synthesis. By carefully controlling the amount of gold precursor and additional capping agent used in the coating process, the gold shell thickness could be controllably tuned, as illustrated by the compositional and structural characterization of the resulting particles.[15] While the absolute shell thickness is difficult to determine for these particles (primarily because of the close lattice match of the two metals, the propensity for an alloy to form at the interface of the Ag and Au metals, and structural imperfections), the relative shell thickness increases as a function of amount of gold precursor used. The resulting NPs were characterized using a wide range of techniques to address the compositional, morphological, structural, and other properties.[15] Table I lists the metallic feeding ratio, moles of Ag, Au, and acrylate used in each synthesis as well as the resulting NP size as determined by TEM and composition as determined by EDS and XPS. The primary difference between the EDS and XPS techniques is that EDS could be used to determine the composition of several different individual particles, then an average could be taken, while for XPS a relatively large beam area results in simultaneous analysis of many particles at the same time. For the sample prepared with 5 % Au atomic feeding ratio, both the EDS and XPS results reflect a total particle composition consistent with the feeding ratio. However, for the cases with 15 and 25 % Au atomic feeding ratio, both EDS and XPS results indicate a heightened amount of gold present in the NPs. This observation is attributed to two primary phenomena. First, some silver will inevitably be lost through etching by gold during the early stages of the coating reaction, and second, both EDS and XPS techniques have finite penetration depths, so that as the gold layer increases in thickness, the compositional results become skewed towards the Au content.[15]

Figure 1 shows a series of TEM images of the synthesized Ag and Ag@Au NPs. Figure 1(a) shows the TEM image for Ag NPs. These particles serve as the cores for further coating with Au. Figure 1(b) shows a sample of Ag@Au NPs synthesized with atomic feeding ratio of 5 % gold. Inspection of the TEM image reveals particles with a uniform spherical morphology.

Figure 1(c) shows a sample of Ag@Au NPs synthesized with an atomic feeding ratio of 15 % gold. The TEM image shows several particles with a spherical morphology, but now several particles are observed that have a lighter spherical center and darker outside ring. The observation of this dark outside and light center is inconsistent among different particles in the sample, some particles display no darker ring and light center at all, or some particles display simply a light spot near the periphery of the NP. We attribute this observation to the formation of an incomplete Au shell on the Ag particle surface. In effect, the round holes that are observed on the particles in the TEM image are a gap or hole in the Au shell, allowing the observation of the Ag core inside the particle. This phenomenon has been observed previously[3)] and likely exists because of the ability of gold to etch away silver.[24,25)] Indeed, some particles display multiple gaps in the Au shell at the particle surface resulting in a unique morphology for the NPs (see Figs. S4 and S5 in ref. 15). If the lighter center and the darker outside ring respectively represent the Ag core and the Au shell with a complete core-shell structure, the atomic ratio of Au to Ag should be much higher than those measured by EDS and XPS (see Table I). It means that the lighter center would be the Ag core partly exposed to outside. In addition a minor fraction (~ 10 %) of small (~ 7 nm) particles are observed in this image. These small particles have a negligible impact on the resulting optical properties (intensity is proportional to R^3, R = particle radius) so are not considered to play a significant role in the resulting UV-vis spectra. Finally, Figure 1(d) shows a sample of Ag@Au NPs synthesized using an atomic feeding ratio of 25 % gold. The TEM image reveals many particles with a light center and thick dark outside. As will be discussed later, this light colored inclusion that exists for a majority of NPs in the TEM image could arise as a result of silver being present in the NP center (appearing lighter in color because Ag is not nearly as dense as Au), or could arise as a void space inclusion within the particle. In addition the particles have adopted roughly hexagonal or pentagonal shapes, reflecting the tendency of Ag nanocrystals to be oriented in the twinned structure, templating the growth of Au at their surface. Note that the observation of

varying image density among different NPs (dark and light spots) in the TEM images occur as a result of many factors, including not only the differences in metal density of Ag and Au but also crystal alignment with the electron beam (explaining why some particles and individual crystalline faces on the particles are completely dark in color while others are light).

Photographs and UV-vis spectra were also collected for the samples of Ag and Ag@Au NPs to study the unique optical properties for these materials. The inset to Fig. 2 shows a photograph for Ag and Ag@Au NPs with Au content increasing from left to right for each sample in the image (Au atomic feeding ratio 0, 5, 15, and 25 % respectively). The Ag particles are a yellow color. The Ag@Au particles with the least addition of Au are a similar yellow color with a barely perceptible amber tone in the sample. Next, the Ag@Au particles with an intermediate addition of Au are a grayish-brown color. Finally the Ag@Au particles with the highest addition of Au are a purple color. These samples were all stable for several months of storage at ambient conditions with no signs of precipitation or changes in the coloring of the solution, which is aided by the removal of the excess reactants after synthesis. The coating of the Ag NPs by Au is also expected to increase the stability as the Au acts as a barrier to the oxidation of the Ag core. This protection is also expected for common conditions in routine biomolecular detection.[1)] Figure 2 shows the UV-vis spectra collected for each sample of Ag and Ag@Au NPs. Spectrum A is for the as-synthesized Ag NPs with SPR peak maximum of 410 nm. Spectrum B is for the Ag@Au NPs with atomic feeding ratio of 5 % Au. While this spectrum also has a peak maximum of 410 nm, the peak intensity has decreased as a result of the suppression of the SPR band by the coating with Au. Spectrum C is for the Ag@Au NPs with atomic feeding ratio of 15 % Au. This spectrum now has two main bands. The primary band at 422 nm has shifted to higher wavelength than that for Ag particles. In addition, the intensity of this band is drastically decreased from that of the earlier samples. A new band has also formed around 600 nm, which is indicative of the increasing amount of Au in the sample being coated on the surface of the Ag particles. Spectrum D is for the Ag@Au NPs with atomic

feeding ratio of 25 % Au, the original Ag peak is now completely obscured, and a long wavelength band has formed at ~610 nm. This long wavelength band for Au is significantly shifted to higher wavelength in the UV-vis spectrum than is typically observed for solid Au NPs of this size (~525 nm).

Finally the dashed line spectrum E is for a sample of NPs in which we purposely formed an alloy. For this sample we added equal amounts of Au and Ag in an identical procedure to the synthesis of Ag NPs (same metal and capping/reducing agent molar amounts/ratio) where the Au and Ag precursors were added simultaneously. The characteristics of this spectrum are different from the other spectra, illustrating the unique optical properties of the Ag@Au NPs. These alloyed Ag-Au NPs (TEM determined size of 10.2 ± 1.5 nm, data not shown) show a peak maximum at 498 nm, in between that for typical Ag and Au monometallic NPs (Ag: ~410 nm, Au: ~525 nm). In addition, the alloy NP sample shows only one peak, whereas the Ag@Au samples show two distinct peaks, the characteristics of which are dependent on the amount of Au added in the coating procedure.

In terms of addressing the core-shell structure of the NPs, one powerful technique that was employed is EDS mapping. In this experiment STEM was used in conjunction with EDS to measure the relative amounts of Ag and Au as a function of two-dimensional space in a single nanoparticle. Figure 3 shows the EDS mapping result for a single Ag@Au NP from those synthesized using atomic feeding ratio of 15 % Au. Figure 3(a) shows a STEM dark field image of the nanoparticle while Fig. 3(b) shows the mapping area of Ag (indicated by the red color, Ag L line), Fig. 3(c) shows the mapping area of Au (indicated by the green color, Au M line), and Fig. 3(d) is an overlay of the two mapping results. As can be clearly observed in the images, a majority of the Ag is located at the center of the particle while the periphery of the NP has a heightened amount of Au. This observation is consistent with a core-shell structure, and reinforces our assertion that these particles are core-shell in nature, despite the presence of some defects in the structure. It is also important to note that the EDS mapping analysis focuses

on a smaller than average particle (~5 nm) to make the visualization of the structure easier, larger particles also show a consistent core-shell structure. The compositional data shows that the individual particles for the various samples all contain silver and gold, while the EDS mapping data illustrates the core-shell nature of the particles.

4. Discussion

In this section, the Mie solution is used to study the optical properties of the synthesized Ag@Au NPs. The results reveal the fine structural properties of the NPs. While a detailed explanation of the Mie modeling is not given here, it has been extensively discussed elsewhere.[16,17] Figure 4 shows the models used with the Mie solution (Mie models) to study the optical properties of the NPs, the corresponding experimental structures associated with each Mie model are also shown. In this work, three Mie models were studied. Model I represents a silver core with a complete coating of gold at the surface that corresponds to an experimental structure with a thin and perhaps non-uniform thickness of gold shell. Model II represents a silver core, surrounded by a void space (water medium) which is completely encapsulated by a gold shell, corresponding to an experimental structure with silver core exposed to the outside environment (water) and incomplete gold shell. Finally, Model III is for a void space encapsulated by a layer of silver which is further encapsulated by a layer of gold. This model corresponds to the experimental structure of a silver core only partially in contact with the gold shell and a void space existing inside the particle. The Mie models used in the calculation were chosen based on the experimentally observed structures for the NPs, and the qualitative correlation between the calculated optical properties for the different models and the experimentally determined ones.

Figure 5 shows two sets of UV-vis spectra modeled using the Mie solution. Figure 5(a) shows spectra for a set of alloy Ag-Au NPs with different composition, while Fig. 5(b) shows the spectra determined for Model I, an Ag@Au structure with a complete layer of gold on the

NP surface and intimate contact between the Ag and Au. In the figure, R_1 is equal to the fraction of the radius composed of Ag while R_2 represents the total radius of the NP including the contribution from Au. As can be observed in the spectra, for the alloy case, the peak maxima lay between that for monometallic Ag and Au NPs, a very well known phenomenon.[17,18,22)] Similarly for the Model I case, the spectra for the Ag@Au NPs lie in between that for the monometallic NPs, which has been observed previously.[17,23)] In addition, a very weak peak at around 240 nm can be observed for the Ag@Au NPs as indicated by the arrow in Fig. 5(b). This weak peak corresponds to the SPR band arising from the Ag-Au interface, and sets the spectrum determined for Model I apart from those of alloy Ag-Au NPs. The results show that for alloyed Ag-Au NPs and Ag@Au NPs with the Model I configuration, the spectra are virtually indistinguishable in terms of elucidating structure. This also reveals the fact that Ag@Au (Model I) NPs should have nearly uniform optical properties, including a single primary peak in the UV-vis spectrum. The band at ~240 nm may arise because of the limitation in the dielectric function described by the simple Drude model ignoring the contribution from interband electron transitions between the valence and conduction bands, and in any case is too weak in intensity to be used to indicate the Ag@Au structure and is not observed in the experimentally collected spectra. It should be noted that this result is in contrast to that obtained in many prior modeling attempts which reported that Ag@Au structures should retain the individual Ag and Au SPR peaks in the absorption spectra with only a dampening of the silver peak as a result of the gold deposition at the surface.[16)] While the calculation approaches used in both the previous and our own studies is nearly identical, the primary difference arises as a result of the dielectric constant used. In the prior work the dielectric constant for bulk Ag and Au materials determined experimentally using electron energy loss spectroscopy (EELS) was used,[16)] while in this work a dielectric constant expressed by the Drude model is used. The Drude model offers an alternate approximation of the dielectric constants for nanoscale particles and so provides an alternate explanation for why a Ag@Au

NP may display two peaks in the UV-vis spectrum. The Drude parameters used in the modeling have a large impact on the resulting spectral features and has found increasing use in other studies with similar results.[17)]

Figure 6 shows two sets of UV-vis spectra calculated using the Mie solution for Ag@Au NPs with different structures. The insets to the spectra show the structure used for the Mie calculation as well as the structural parameters used. Figure 6(a) shows a set of spectra for Ag@Au NPs with an Ag core separated from the Au shell by a void space (Model II). For Fig. 6(a), R_1 is the fraction of the radius occupied by Ag, R_2 includes the radius covered by Ag and the void space, and finally R_3 represents the total radius of the particle, including the contribution from Au. The spectra calculated for the Model II Ag@Au NPs are generally more complex than for Model I. In general, these spectra show two primary peaks, the first ranging between ~400-500 nm attributed to the Ag core component of the structure, and the second ranging from ~650-900 nm attributed to the gold shell component. The weak shoulder peak ranging between ~200-350 nm is attributed to the SPR band arising from the inner surface of the gold shell. This peak (observed for all the core-shell samples) may be an artifact that arises as a result of the limitation in the dielectric function described by the simple Drude model as discussed above. Therefore, the low wavelength peak is not used to address the core-shell structure and is not observed in the experimentally collected spectra. As the size of the isolated silver particle at the center of the structure is increased, the spectral component from silver becomes more predominant while the gold component decreases in intensity and shifts to higher wavelength. Figure 6(b) shows a set of spectra for Ag@Au NPs with a central void space, then a layer of silver coated by a layer of gold (Model III). In Fig. 6(b), R_1 is the fraction of the radius covered by the void space, R_2 includes the fraction of the radius covered by the void space plus Ag, and finally R_3 is the total radius including Au. For the case of Model III, each spectrum shows two main components. Two low intensity peaks are observed in the range of ~200-300 nm (contributions from the Ag-Au interface and the inner surface of silver, as

predicted by the Mie Model), while a primary peak (contribution from the outer surface of gold) exists in the range of ~500-700 nm. This intense peak shifts to higher wavelength and decreases in intensity as the void space is increased in size and the gold layer is decreased in thickness.

Finally, the experimentally collected optical properties for the Ag@Au NPs are correlated to those calculated using the Mie solution. Figure 7 shows the UV-vis spectra for each of the three different compositions of Ag@Au NPs synthesized along with the qualitatively closest matching UV-vis spectrum calculated using the Mie solution. The insets to Fig. 7 show the model structure used and the corresponding HR-TEM image for an individual Ag@Au NP exhibiting the experimental core-shell structure. For the Ag@Au NPs synthesized with atomic feeding ratio of 5 % Au [Fig. 7(a)], Model I with parameters of $R_1 = 0.7$ and $R_2 = 1$ shows the best fit, which is not surprising given the small amount of gold used in the synthesis. It is likely that the gold is dispersed over the Ag core as a sub-monolayer because 5 % feeding ratio of Au is not sufficient for a complete coating. The sub-layer of Au is completely coupled to the Ag surface leading to uniform optical properties. For the Ag@Au NPs with atomic feeding ratio of 15 % Au [Fig. 7(b)], Model II with parameters of $R_1 = 0.3$, $R_2 = 0.45$, and $R_3 = 1$ provides the best fit (though the calculated and experimental spectra do show some deviation, it is the spectral features that we base the fitting on). This reflects the fact that some particles display gaps in the Au coating, exposing the inner silver, causing two peaks to be observed in the UV-vis spectrum for this sample. Finally for the Ag@Au NPs with atomic feeding ratio of 25 % Au [Fig. 7(c)], Model III with parameters of $R_1 = 0.6$, $R_2 = 0.8$, and $R_3 = 1$ shows the best fit. This reflects the action of gold etching away some of the silver core leaving a void space within the particle, with gold eventually forming a complete shell over the core area. It is important to note that the calculated and experimental spectra, particularly in Figs. 7(b) and 7(c), show significant deviation in the spectral fitting. This arises from a combination of several factors including the fact that the as-synthesized NPs are not monodisperse, the core-shell structures are not uniform among all the different particles in the sample (i.e., there is likely

some shell thickness deviation among different particles), and there is the possibility of some alloy formation at the gold and silver interface in the particles, which is ignored using Mie Modeling. Despite this, the calculated and experimental spectral characteristics are qualitatively consistent, with both calculated and experimentally collected spectra indicating the various core-shell structures discussed. Another important aspect of the calculated spectra is that the volume ratio of Au calculated from the model parameters is always much larger than that estimated from EDS, XPS and the experimental feeding ratio of Au to Ag. This discrepancy might be caused by the differences between the models and the real structures in the Ag@Au NPs, i.e. our model structures would need to be oversimplified to obtain a quantitative agreement. Nonetheless, these simple models can reproduce the complicated optical properties of the experimentally synthesized Ag@Au NPs, that is, two strong peaks are observed for 15 % Au with the longer-wavelength peak found around 600 nm, which is significantly red-shifted compared to the SPR band of solid Au NPs (525 nm), or a single long-wavelength peak is observed for 25 % Au, which is also significantly red-shifted compared to the SPR band of solid Au NPs. In both cases, the incorporation of a silver/medium interface in the model results in the optical behavior observed experimentally.

These observations are intriguing and indicate a gradual change in structure and optical properties as more Au is added in the coating experiment. One of the greatest (and extensively discussed) challenges in the preparation of Ag@Au NPs is the relative reduction potential of the two metals. In short, the higher reduction potential of Au means that if Au ions are added to Ag metal, the Au will be reduced to metallic state at the expense of Ag metal which is oxidized. In fact this has been taken advantage of by Sun *et al.* to create Au NPs with unique and interesting shapes.[24] The phenomenon often causes the formation of either hollow Au spheres, or alloyed Ag-Au NPs, whose properties deviate markedly from that for Ag@Au NPs.[22] In the coating procedure described here, as Au is added to the Ag NPs, it is reduced at the surface of the Ag NP and some Ag is inevitably etched away. In the synthetic approach this effect is

suppressed by adding acrylate as a reducing agent to protect etching of the Ag core. Despite this, as more Au is added, the etching effect of Au on Ag metal is accentuated. Realistically speaking, for addition of 5 % Au in the coating procedure, too little Au is present to cause an observable etching effect. For 15 % Au, the etching produces a gap or hole in the Au shell to allow Ag to escape the core of the particle, while for 25 % addition of Au enough Ag has been etched away to leave a void space in the particle core, with enough Au present to completely form over the gap. Despite these observations, it is important to note that for 25 % addition of Au, there is enough Au present stoichiometrically to completely etch away all Ag in the sample, however both EDS and XPS results show the presence of Ag remaining in the particles. This illustrates the ability of acrylate reducing agent to at least partially suppress the etching effect. The collective results strongly suggest that as Au is added in the coating of the Ag particles the structure gradually changes from that of Ag NPs uniformly coated by a thin layer of Au, to particles with a gap or hole in the Au shell, to particles with a combination of Ag/void space in the center.

5. Conclusions

In this study the optical properties of a set of Ag@Au NPs composed of different amounts of Au are correlated to those calculated using the Mie solution for an idealized set of structures. The results indicate that the as-synthesized materials have a discrete core-shell structure, but there are defects present depending on the amount of gold added in the coating procedure, which has a large impact on the resulting optical properties. In general for the case of atomic feeding ratio of 5 % Au, the optical properties indicate a uniform and thin coating of gold on the silver core. For the case of atomic feeding ratio of 15 % Au, the optical properties suggest particles with gaps in the gold shell, consistent with TEM observations. Finally for atomic feeding ratio of 25 % Au, the optical properties suggest a void space within the particles. These observations reveal the evolution of the Ag@Au structure as increasing amounts of Au are

added in the coating procedure. Importantly, even by using an ultra-high resolution STEM, we could not clearly see an interfacial structure of Ag@Au nanoparticles. It turns out that the Mie solution for Ag@Au NPs with non ideal structures would be a good tool to get an insight into the microstructure of shell which can not be easily addressed from two-dimensional microscopic images. The results lend insight into the design and synthesis of metallic nanoprobes with desired and controllable optical properties for applications in sensing and medical diagnostics.

Acknowledgments

Derrick Mott gratefully acknowledges support by the Japan Society for the Promotion of Science (JSPS) fellowship. We thank Dr. Jinwang Li for his assistance in the use of TGA instrumentation, Nobuaki Ito for assistance in the use of XPS instrumentation, and Koichi Higashimine for assistance in the use of STEM and HR-TEM instrumentation.

References

1) N. L. Rosi and C. A. Mirkin: Chem. Rev. **105** (2005) 1547.

2) I-I. S. Lim, D. Mott, M. H. Engelhard, Y. Pan, S. Kamodia, J. Luo, P. N. Njoki, S. Zhou, L. Wang, and C-J. Zhong: Anal. Chem. **81** (2009) 689.

3) Y. Cui, B. Ren, J-L. Yao, R-A. Gu, and Z-Q. Tian: J. Phys. Chem. B **110** (2006) 4002.

4) Y-W. Cao, R. Jin, and C. A. Mirkin: J. Am. Chem. Soc. **123** (2001) 7961.

5) A. Tcherniak, J. W. Ha, S. Dominguez-Medina, L. S. Slaughter, and S. Link: Nano Lett. **10** (2010) 1398.

6) S. Nie and S. R. Emory: Science **275** (1997) 1102.

7) I-I. S. Lim, U. Chandrachud, L. Wang, S. Gal, and C-J. Zhong: Anal. Chem. **80** (2008) 6038.

8) C-C. Huang, Z. Yang, and H-T. Chang: Langmuir **20** (2004) 6089.

9) S. Xu, B. Zhao, W. Xu, and Y. Fan: Colloids Surf. A **257** (2005) 313.

10) Y. Yang, X. Gong, H. Zeng, L. Zhang, X. Zhang, C. Zou, and S. Huang: J. Phys. Chem. C **114** (2010) 256.

11) L. Lu, A. Kobayashi, K. Tawa, and Y. Ozaki: Chem. Mater. **18** (2006) 4894.

12) I. Srnova-Sloufova, F. Lednicky, A. Gemperle, and J. Gemperlova: Langmuir **16** (2000) 9928.

13) J. Yang, J. Y. Lee, and H-P. Too: J. Phys. Chem. B **109** (2005) 19208.

14) I. Hussain, M. Brust, A. J. Papworth, and A. I. Cooper: Langmuir **19** (2003) 4831.

15) D. Mott, N. T. B. Thuy, Y. Aoki, and S. Maenosono: Philos. Trans. R. Soc. A **368** (2010) 4275.

16) P. Mulvaney: Langmuir **12** (1996) 788.

17) J. Zhu: Physica E **27** (2005) 296.

18) S. Link, Z. L. Wang, and M. A. El-Sayed: J. Phys. Chem. B **103** (1999) 3529.

19) P. Billaud, J-R. Huntzinger, E. Cottancin, J. Lermé, M. Pellarin, L. Arnaud, M. Broyer, N.

Del Fatti, and F. Vallée: Eur. Phys. J. D **43** (2007) 271.

20) K. L. Kelly, E. Coronado, L. L. Zhao, and G. C. Schatz: J. Phys. Chem. B **107** (2003) 668.

21) P. N. Njoki, I-I. S. Lim, D. Mott, H-Y. Park, B. Khan, S. Mishra, R. Sujakumar, J. Luo, and C-J. Zhong: J. Phys. Chem. C **111** (2007) 14664.

22) M. Gellner, B. Küstner, and S. Schlücker: Vib. Spectrosc. **50** (2009) 43.

23) R. Ferrando, J. Jellinek, and R. L. Johnston: Chem. Rev. **108** (2008) 847.

24) Y. Sun and Y. Xia: Anal. Chem. **74** (2002) 5297.

25) Y. Sun and Y. Xia: J. Am. Chem. Soc. **126** (2004) 3892.

Figure captions

Fig. 1. TEM images Ag NPs (a), and Ag@Au NPs with atomic feeding ratio of: 5 % Au (b), 15 % Au (c), and 25 % Au (d).

Fig. 2. (Color online) UV-vis spectra for Ag and Ag@Au NPs prepared with increasing Au content, as-synthesized Ag NPs (a), 5 % Au atomic feeding ratio (b), 15 % Au atomic feeding ratio (c), 25 % Au atomic feeding ratio (d), and a Ag-Au NP alloy (e). The inset shows the photographs of the Ag and Ag@Au NPs.

Fig. 3. (Color online) High-angle annular dark-field STEM image (a) and EDS mapping of Ag (b) and Au (c) in a single NP. The overlay image (d) shows the relative location of Ag and Au in a single NP. The scale bar applies to all images.

Fig. 4. (Color online) The Mie Model structures of Ag@Au NPs used with the Mie solution along with the corresponding experimental structures.

Fig. 5. (Color online) UV-vis spectra calculated using the Mie solution for alloy Ag-Au NPs (a), and for Ag@Au NPs with the Model I structure (b).

Fig. 6. (Color online) UV-vis spectra calculated using the Mie solution for Ag@Au NPs using Model II (a), and for Ag@Au NPs using Model III (b).

Fig. 7. (Color online) UV-vis spectra (solid line) for the three different types of Ag@Au NPs synthesized along with the corresponding best fit spectra calculated using the Mie solution (dashed line) for atomic feeding ratio of 5 % Au and Model I (a), atomic feeding ratio of 15 % Au and Model II (b), and atomic feeding ratio of 25 % Au and Model III (c), respectively. The

insets to the spectra represent the model used for the calculation along with the corresponding HR-TEM image of a single representative NP from each sample exhibiting the correlated structure.

Table I. Metallic feeding ratio, moles of Ag, Au and acrylate, TEM determined size and EDS/XPS determined compositions for Ag and Ag@Au nanoparticle samples.

Feeding ratio	Ag (mol)	Au (mol)	Acrylate (mol)	TEM size (nm)	EDS	XPS
Ag_{100}	1.25×10^{-5}	0	2.55×10^{-4}	20.5±3.2	Ag_{100}	Ag_{100}
$Ag_{95}Au_5$	1.25×10^{-5}	6.25×10^{-7}	1.38×10^{-4}	17.5±3.7	$Ag_{93.0}Au_{7.0}$	$Ag_{94.8}Au_{5.2}$
$Ag_{85}Au_{15}$	1.25×10^{-5}	1.88×10^{-6}	1.38×10^{-4}	16.3±2.7	$Ag_{60.6}Au_{39.4}$	$Ag_{57.7}Au_{42.3}$
$Ag_{75}Au_{25}$	1.25×10^{-5}	3.13×10^{-6}	1.38×10^{-4}	17.5±5.1	$Ag_{50.8}Au_{49.2}$	$Ag_{60.6}Au_{39.4}$

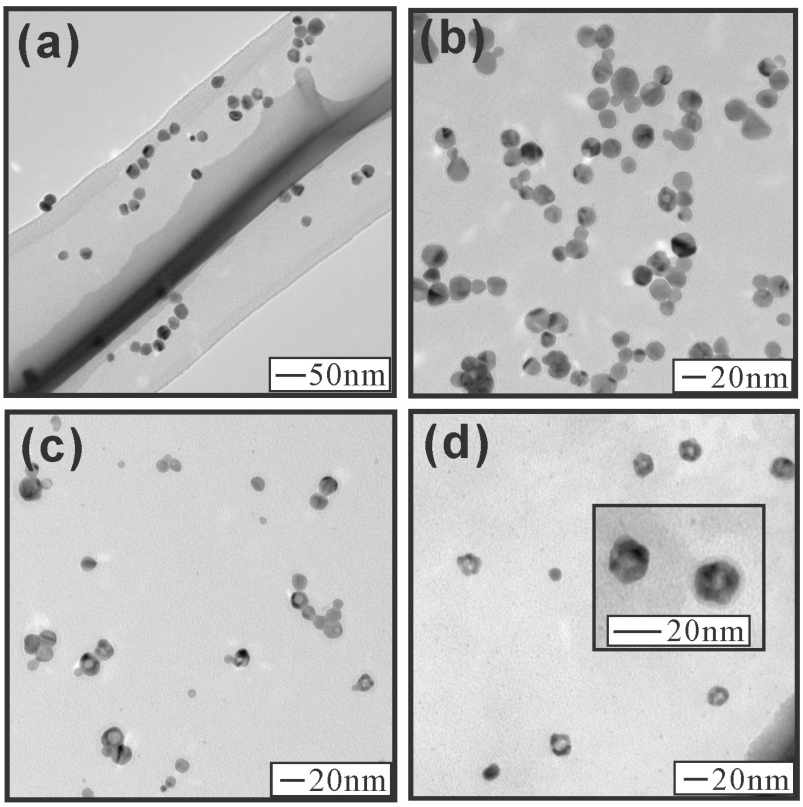

Fig. 1. TEM images Ag NPs (a), and Ag@Au NPs with atomic feeding ratio of: 5 % Au (b), 15 % Au (c), and 25 % Au (d).

D. Mott *et al.*

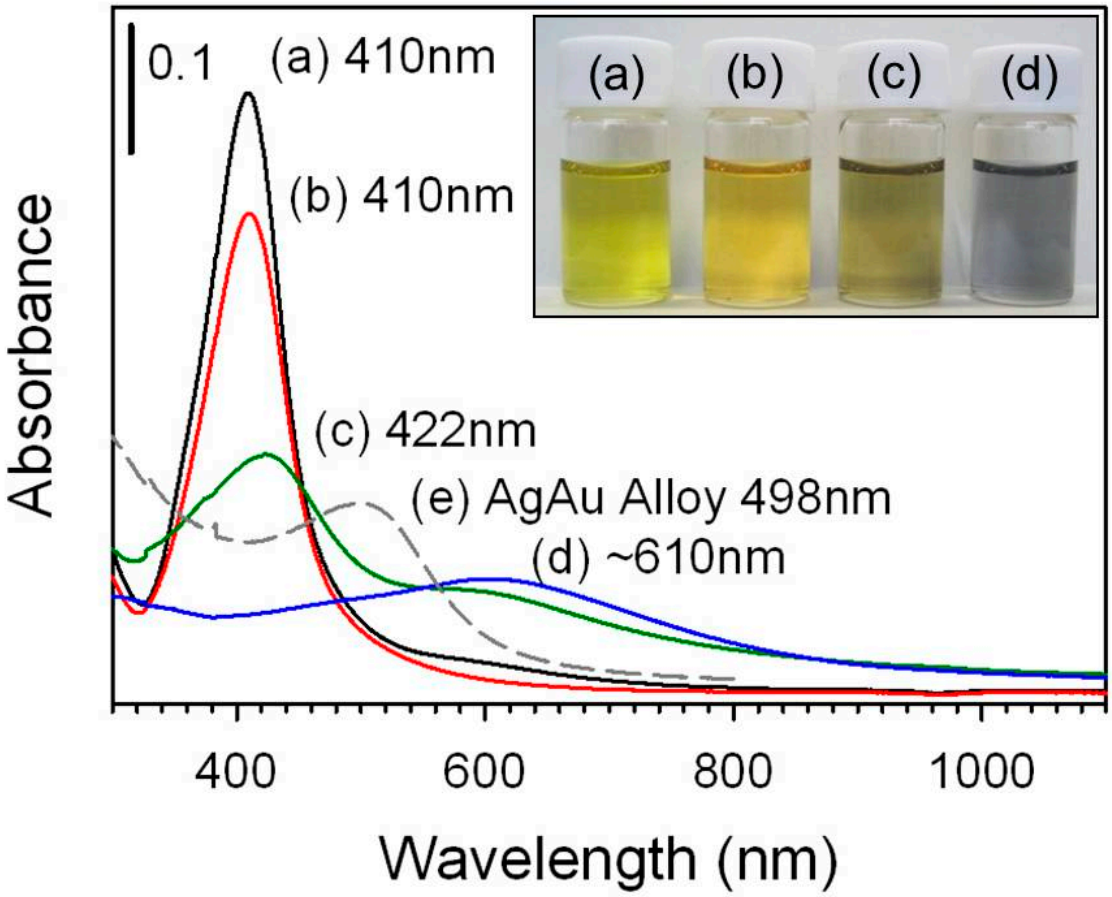

Fig. 2. UV-vis spectra for Ag and Ag@Au NPs prepared with increasing Au content, as-synthesized Ag NPs (a), 5 % Au atomic feeding ratio (b), 15 % Au atomic feeding ratio (c), 25 % Au atomic feeding ratio (d), and a Ag-Au NP alloy (e). The inset shows the photographs of the Ag and Ag@Au NPs.

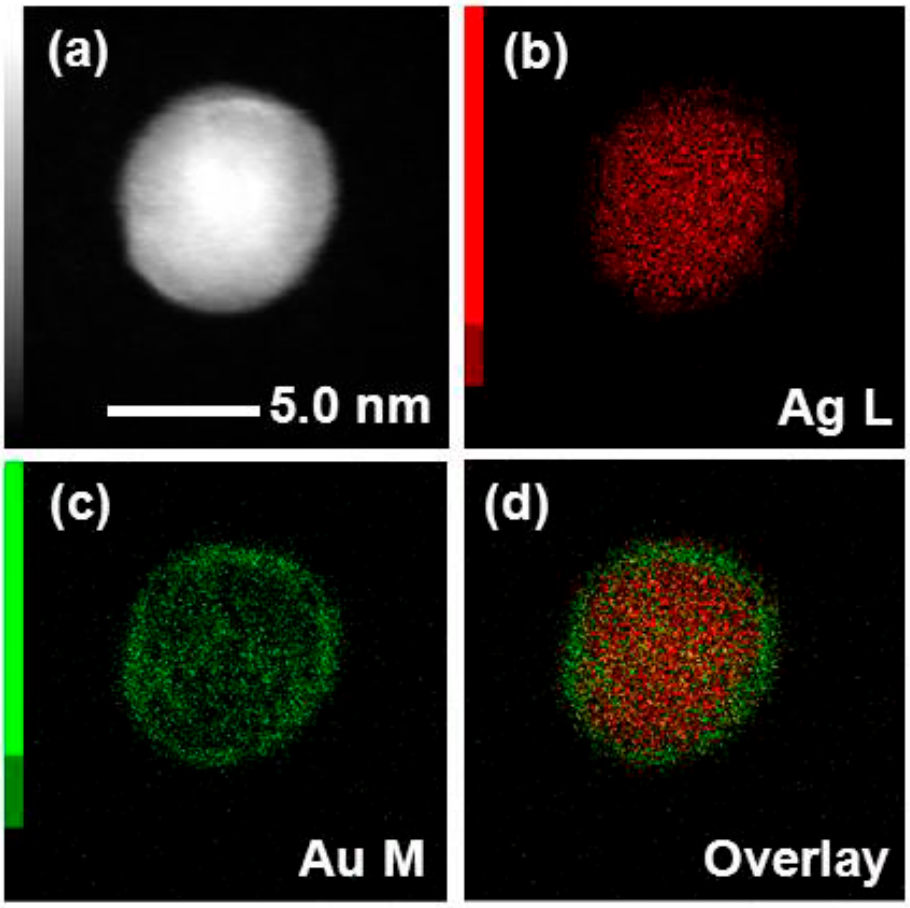

Fig. 3. High-angle annular dark-field STEM image (a) and EDS mapping of Ag (b) and Au (c) in a single NP. The overlay image (d) shows the relative location of Ag and Au in a single NP. The scale bar applies to all images.

D. Mott *et al.*

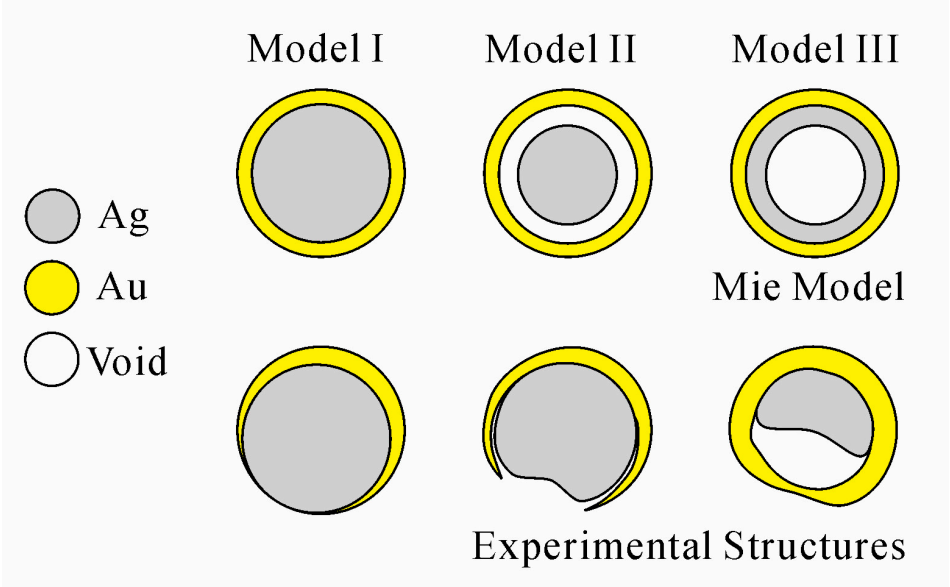

Fig. 4. The Mie Model structures of Ag@Au NPs used with the Mie solution along with the corresponding experimental structures.

D. Mott *et al.*

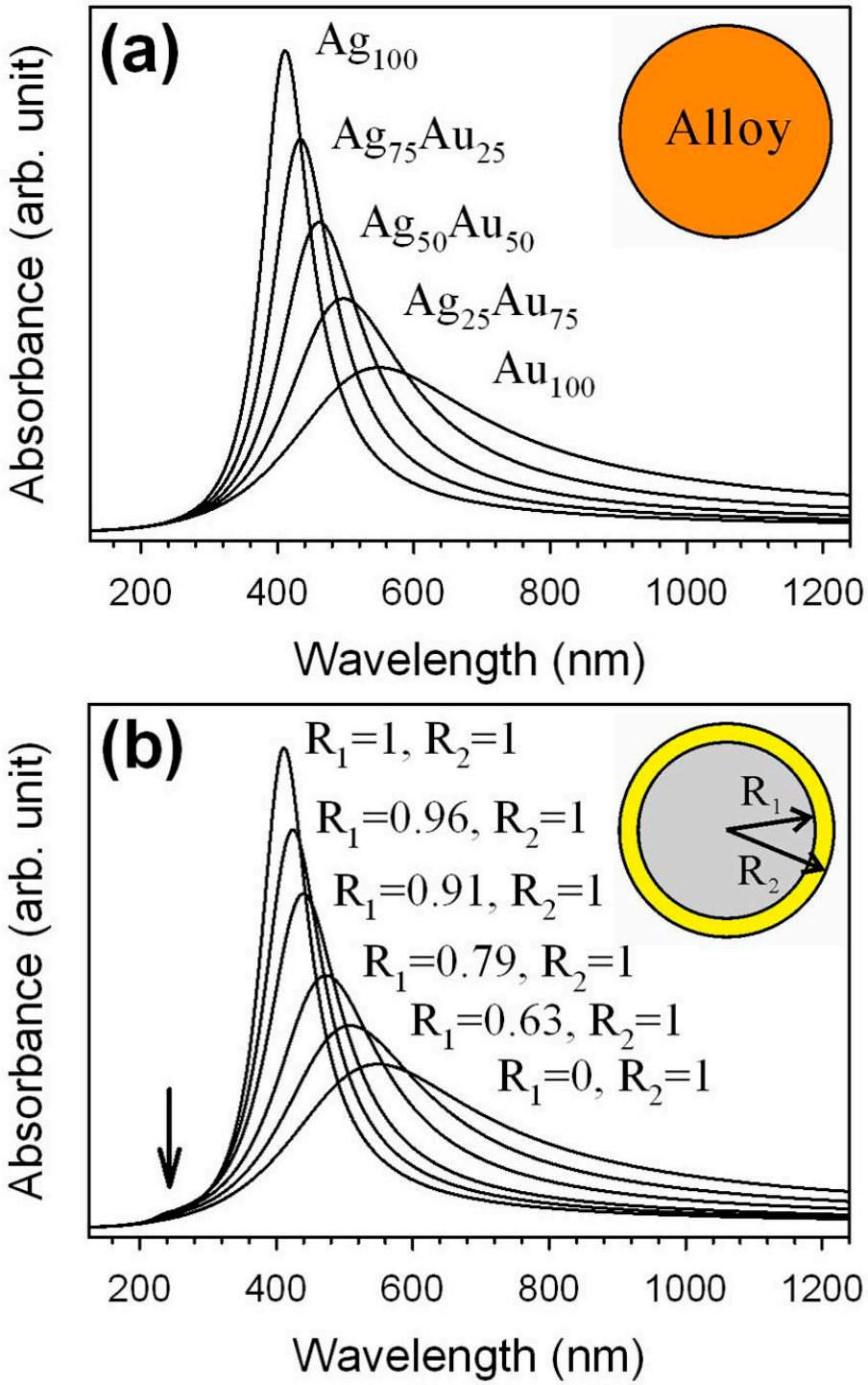

Fig. 5. UV-vis spectra calculated using the Mie solution for alloy Ag-Au NPs (a), and for Ag@Au NPs with the Model I structure (b).

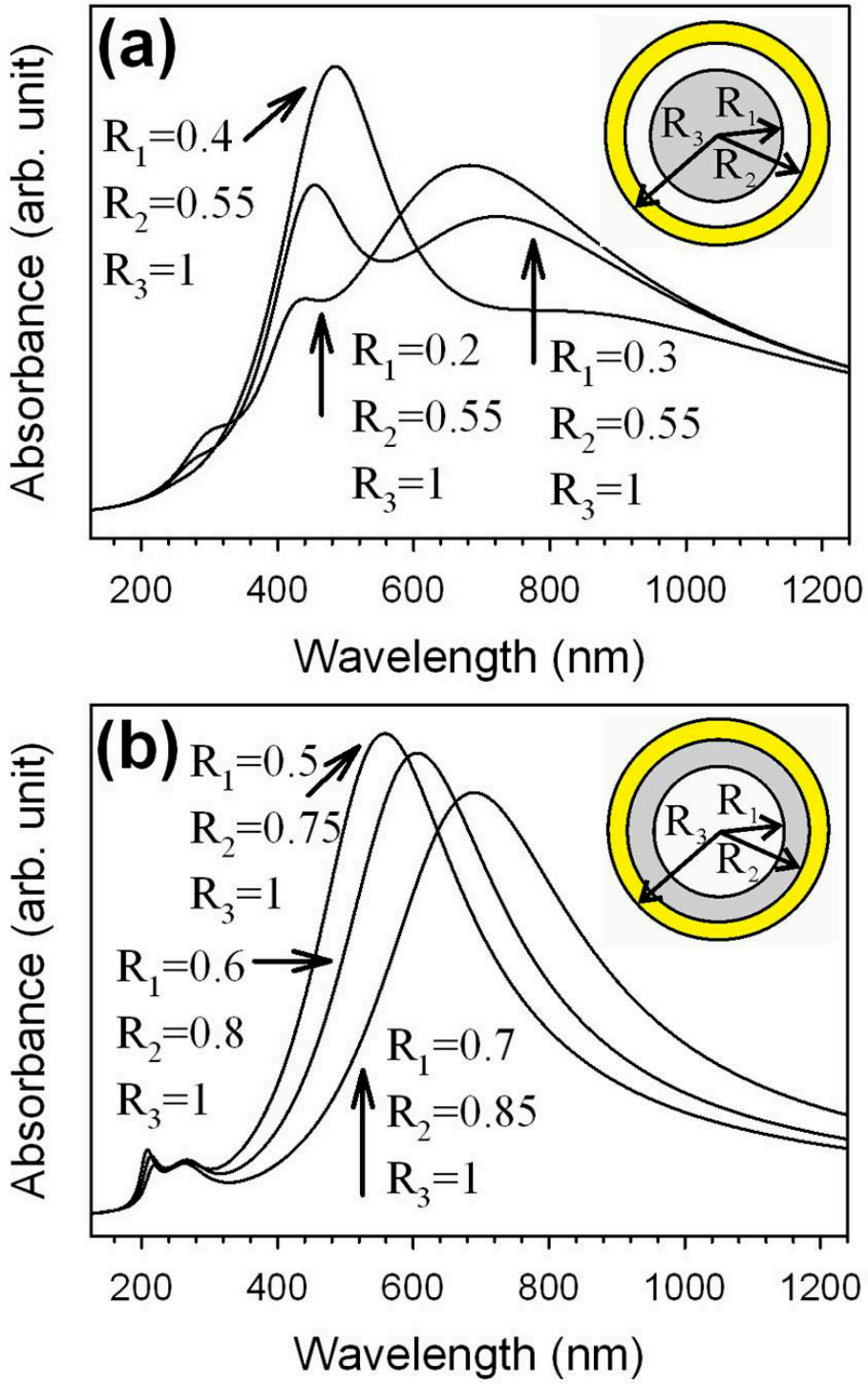

Fig. 6. UV-vis spectra calculated using the Mie solution for Ag@Au NPs using Model II (a), and for Ag@Au NPs using Model III (b).

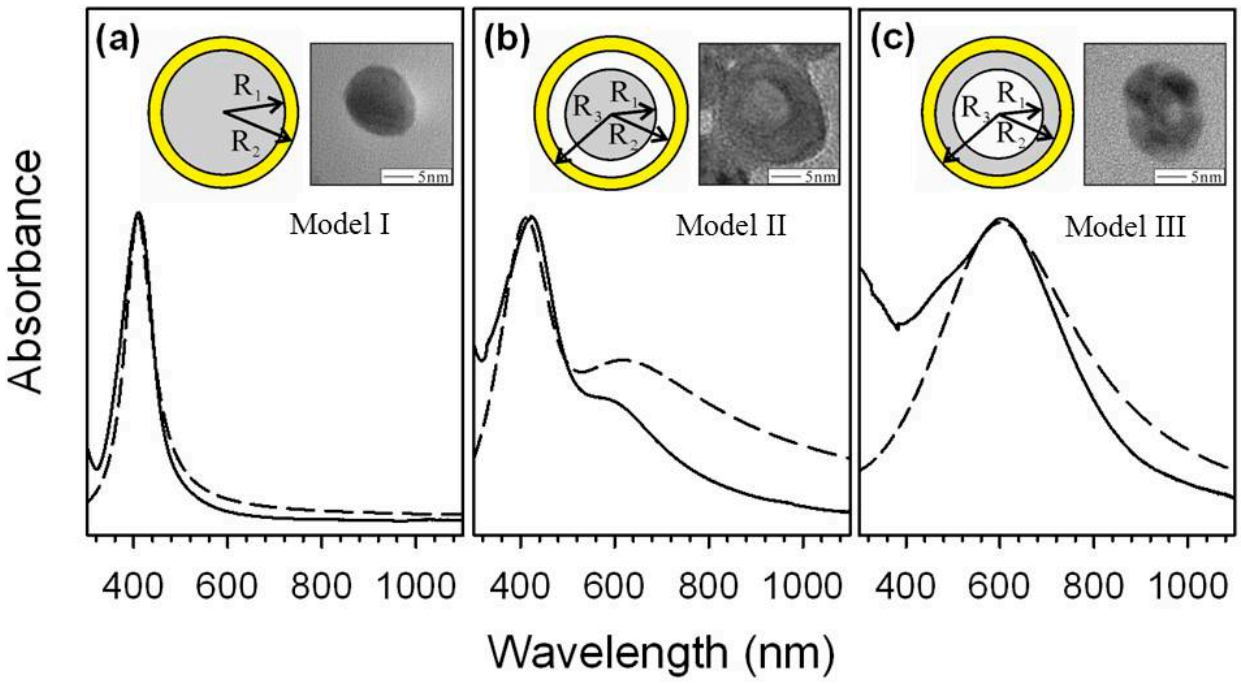

Fig. 7. UV-vis spectra (solid line) for the three different types of Ag@Au NPs synthesized along with the corresponding best fit spectra calculated using the Mie solution (dashed line) for atomic feeding ratio of 5 % Au and Model I (a), atomic feeding ratio of 15 % Au and Model II (b), and atomic feeding ratio of 25 % Au and Model III (c), respectively. The insets to the spectra represent the model used for the calculation along with the corresponding HR-TEM image of a single representative NP from each sample exhibiting the correlated structure.